PROCEEDINGS OF MOSES2023 CONFERENCE
4TH INTERNATIONAL CONFERENCE ON MODELLING AND OPTIMISATION OF SHIP ENERGY SYSTEMS
26-27 OCTOBER 2023, DELFT, NETHERLANDS

Evaluation of Methanol Sprays in Marine Internal Combustion Engines: a Case Study for Port Fuel Injection Systems

Konstantinos Zoumpourlos[a,*], Andrea Coraddu[a], Rinze Geertsma[a,b], and Robert van de Ketterij[b]

[a]Delft University of Technology, Delft, Netherlands
[b]Netherlands Defence Academy, Den Helder, Netherlands
[*]k.zoumpourlos@tudelft.nl

Abstract

Methanol has emerged as a cost-effective and scalable alternative fuel for the maritime sector. However, the use of methanol in marine engines is limited by the unknown characteristics of methanol sprays when introduced through retrofitted port fuel injection (PFI) systems. The present study investigates the characteristics of methanol sprays under relevant conditions for marine engines, such as low injection pressure PFI. The primary objective of this research is to advance knowledge into key spray characteristics, including spray penetration, droplet size, atomization quality, and evaporation. The proposed methodology evaluates the efficacy of state-of-the-art computational fluid dynamics (CFD) models in simulating PFI marine engine spray conditions. Moreover, the study compares the performance of the Kelvin-Helmholtz (KH-RT) and Taylor Analogy Breakup (TAB) droplet breakup models under low injection pressure conditions. The results demonstrated that the KH-RT model does not predict any droplet breakup occurrence suggesting that the TAB model is more suitable for the given conditions. Furthermore, the liquid penetration of the spray was observed to align with the outcomes reported in previous experimental literature on methanol sprays. Nevertheless, the droplet sizes for low pressure injectors appear relatively large, indicating poor spray atomization, which impedes rapid evaporation and increases the risk of wall wetting in the inlet manifold and combustion chamber.

Keywords: Methanol; Internal Combustion Engine; Computational Fluid Dynamics; Spray Penetration; Droplet Size; Atomization Quality; Evaporation.

1 INTRODUCTION

Increased greenhouse gas emissions from the maritime industry contribute to climate change [1]. These emissions are mostly produced during the combustion of fossil fuels in internal combustion engines (ICEs) that are used for power and propulsion [2]. To address this issue, there is a growing need to shift towards sustainable energy solutions, such as electrified propulsion [3], [4]. However, most of these energy solutions are not yet mature enough for implementation at a scale due to their low energy density and range limitation, therefore enlarging the reliance on ICEs [3], [5], [6]. Hence, to reduce emissions, leveraging alternative fuels is urgent to decarbonize ICE-powered vessels [7], [8].

Methanol is identified as a potential alternative fuel for the maritime sector, demonstrating scalable production, adequate properties, and low cost [9], [10]. Moreover, the integration of methanol in state-of-the-art marine ICEs is achieved through different injection strategies, namely port fuel injection (PFI) and direct injection (DI) [9], [11]. Among these techniques, PFI systems are commonly favored in the maritime sector as an easy retrofitting solution for existing natural gas and diesel engines [9], [12]. These systems introduce fuel into the engine's intake manifold and are preferred because of their affordability and simple installation process [9].

However, integrating methanol into marine ICEs presents a significant challenge owing to its high latent heat of vaporisation [9]. Compared to diesel, methanol exhibits nearly half the lower heating value, adding another degree of complexity to its integration [11], [13], [14]. Consequently, longer injection duration and increased mass quantities are required to achieve the same power output. In addition, operation under PFI conditions is limiting because of the unknown characteristics of methanol sprays [9]. Therefore, a thorough understanding of methanol's injection and evaporation process is crucial for comprehending its combustion characteristics and emissions.

This study examines the impact of methanol PFI

DOI: https://doi.org/10.59490/moses.2023.655

systems on spray characteristics and evaporation. The methodology involves computational fluid dynamics (CFD) modeling, with validation from dedicated spray experiments under PFI conditions [15]. Moreover, the efficacy of state-of-the-art spray models was evaluated, leading to selecting of the most appropriate droplet breakup and turbulence models. Particularly, under PFI conditions, the droplet interactions with the surrounding ambient air differ significantly from DI sprays. This differentiation arises from the fact that the ambient pressure and temperature conditions impose less intensive interactions between the liquid spray and the ambient air. Hence, using CFD, methanol spray behaviour in PFI conditions can be studied and analyzed in detail.

The paper is structured as follows. Section 2 provides a concise overview of the literature and the problem related to low-pressure methanol PFI sprays. In Section 3, the CFD numerical methodology is described in detail. Furthermore, Section 4 presents the experimental conditions on which the model is based, including information on the initial and boundary conditions and the employed computational mesh. The comparison of turbulence and breakup models, along with relevant discussions on the performance of each model, is presented in Section 5. Finally, Section 6 provides the conclusions drawn from the study.

2 PROBLEM STATEMENT & RELATED WORK

The phase transition process of methanol presents unique thermodynamic properties, necessitating an elevated amount of thermal energy for evaporation compared to traditional fuels. This phenomenon is attributable to its significantly higher latent heat of vaporization: $h_{lg,MeOH} \approx 4 \cdot h_{lg,Diesel}$ as reported in [9]. Considering also methanol's lower heating value being half that of diesel, approximately eight times the amount of thermal energy is required for complete evaporation while maintaining the same power output. Experimental research in this domain has been predominantly confined to DI conditions, which are characterized by high ambient and injection pressures, along with high temperature [16]–[19]. Particularly, these experimental efforts have tried to characterize spray parameters such as penetration length, cone angle and vapor penetration under these conditions. Consequently, a knowledge gap exists on the behavior of methanol sprays at inlet manifold conditions, predominantly characterized by near atmospheric ambient conditions coupled with low injection pressures. Further research is required to fill this gap, which would contribute to a better understanding of the fuel-air mixture formation process in methanol engines.

Previous research on conventional fuels demonstrated that certain spray sub-models and boundary conditions such as the liquid droplet breakup model, the turbulence model [20]–[22], and the mass Rate Of Injection (ROI) [23] significantly affect the transient response of the spray. However, under low injection pressure, it is still unclear whether the state-of-the-art models can accurately predict spray penetration and droplet breakup.

A factor that is greatly affecting the breakup behavior of the droplets is the Weber (We) number, which is the ratio of the aerodynamic drag force imposed from the ambient air onto the droplet and the droplet surface tension force [24]:

$$\mathrm{We} = \frac{\rho_g u^2 r_d}{\sigma} \tag{1}$$

where ρ_g is the ambient air density, u is the droplet velocity, r_d is the droplet radius, and σ is the droplet surface tension. Since the Weber number of low injection pressure sprays is significantly lower than in high pressure sprays, the droplet surface tension significantly impacts the liquid breakup submodel and, therefore, the liquid penetration [25], [26]. Hence, this research aims to investigate the influence of the Taylor Analogy Breakup (TAB) model [24], which is recommended for low Weber number droplets in the vibrational breakup mode [27]. Consequently, the TAB model was compared with the Kelvin Helmholtz - Rayleigh Taylor (KH-RT) model [28], which is widely adopted in DI spray research.

3 NUMERICAL SETUP

This computational study employed the commercial CONVERGE v3.0 CFD code [29], which contains a framework for the numerical analysis of multiphase flow studies. The framework utilizes the finite volume approach to solve the compressible conservation equations of mass, momentum, and energy, coupled with a variable time-step control algorithm based on the Courant-Friedrichs-Lewy (CFL) criterion [30]–[32]. The conservation of mass, momentum, and energy are formulated according to Equations 2, 3, and 5 respectively:

$$\frac{\partial \rho}{\partial t} + \frac{\partial (\rho u_i)}{\partial x_i} = 0 \tag{2}$$

$$\frac{\partial(\rho u_i)}{\partial t} + \frac{\partial}{\partial x_j}[\rho u_i u_j + P\delta_{ij} - \sigma_{ij}] = 0 \quad (3)$$

where σ is the viscous stress tensor

$$\sigma_{ij} = \mu(\frac{\partial u_i}{\partial x_j} + \frac{\partial u_j}{\partial x_i}) + (\mu_\nu - \frac{2}{3}\mu)\frac{\partial u_k}{\partial x_k}\delta_{ij} \quad (4)$$

$$\frac{\partial(\rho e_0)}{\partial t} + \frac{\partial}{\partial x_j}[\rho u_j e_0 + u_j P - K\frac{\partial T}{\partial x_j} - u_i\sigma_{ij} - \rho\sum_m D_m h_m \frac{\partial Y_m}{\partial x_j}] = 0 \quad (5)$$

where the total specific energy is $e_0 \equiv e + \frac{u_k u_k}{2}$, ρ is the fluid density, u is the velocity in each axis, P is the pressure, μ is the viscosity, μ_ν is the dilatational viscosity (set to zero), δ_{ij} is the Kronecker delta, T is the temperature, K is the thermal conductivity, m are the species, Y_m is the mass fraction of species, D_m is the species mass diffusion coefficient, and h_m is the species specific enthalpy.

Moreover, the density-based solver [30] was utilized using the Pressure Implicit with Splitting of Operators (PISO) method [33]. The fluids comprising the simulation, including air and methanol, were modeled based on the Redlich-Kwong equation of state [34]. Finally, the simulations were run in parallel utilizing the DelftBlue supercomputer [35] with the Message Passing Interface (MPI) [36]. An advantageous feature of CONVERGE is its scalability to many cores, resulting in a substantial acceleration in the solution process [30].

Regarding turbulence modeling, the present study employed the RNG and the Standard $k-\epsilon$ turbulence models in the modeling process [37]. Those $k-\epsilon$ models are based on the Reynolds-Averaged-Navier-Stokes (RANS) equations which approximate the velocity field as a summation of a mean and a fluctuating velocity ($u = \bar{u} + u'$). The result of this assumption generates a turbulence induced Reynolds-stress tensor in the Navier-Stokes equations. Resolving the stress tensor leads to modeling two additional transport equations accounting for the turbulent kinetic energy (k), and the rate of dissipation of turbulent kinetic energy (ϵ) [32], [38]. The transport equations for k and ϵ are as follows [30]

$$\frac{\partial(\rho k)}{\partial t} + \frac{\partial(\rho u_i k)}{\partial x_i} = \tau_{ij}\frac{\partial u_i}{\partial x_j} + \frac{\partial}{\partial x_j}\frac{\mu + \mu_t}{Pr_k}\frac{\partial k}{\partial x_j} - \rho\epsilon \quad (6)$$

and

$$\frac{\partial(\rho\epsilon)}{\partial t} + \frac{\partial(\rho u_i \epsilon)}{\partial x_i} = \frac{\partial}{\partial x_j}\left(\frac{\mu + \mu_t}{Pr_\epsilon}\frac{\partial \epsilon}{\partial x_j}\right) + C_{\epsilon 3}\rho\epsilon\frac{\partial u_i}{\partial x_i} + (C_{\epsilon 1}\frac{\partial u_i}{\partial x_j}\tau_{ij} - C_{\epsilon 2}\rho\epsilon)\frac{\epsilon}{k} - \rho R_\epsilon \quad (7)$$

where ρ is the fluid density, u is the velocity in each axis, τ_{ij} is the modeled Reynolds stress, μ is the viscosity, μ_t is the turbulent viscosity, Pr is the Prandtl number, $C_{\epsilon 1}, C_{\epsilon 2}$, and $C_{\epsilon 3}$ are turbulence model parameters.

Additionally,

$$k = \frac{1}{2}\overline{u_i' u_i'}, \quad (8)$$

$$\mu_t = C_\mu \rho \frac{k^2}{\epsilon}, \quad (9)$$

and

$$R_\epsilon = \frac{C_\mu \eta^3(1 - \eta/\eta_0)}{1 + \beta\eta^3}\frac{\epsilon^2}{k} \quad (10)$$

where C_μ, η, η_0 and β are turbulence model parameters. For the Standard $k-\epsilon$ model the last term $R_\epsilon = 0$.

The Lagrangian Particle Tracking (LPT) technique was utilized for modeling the multiphase flow through a Lagrangian-Eulerian (LE) two-way coupling approach [39], [40]. The LPT technique treats the liquid droplets as Lagrangian particles tracked based on their position in the computational domain. On the contrary, the gaseous phase is treated using an Eulerian representation, which treats the flow parameters based on a fixed mesh grid. The coupling between the droplets and the surrounding gaseous medium is ensured through the exchange of momentum, energy (heat transfer), and mass (evaporation) [39]. In addition, various phenomenological sub-grid models are implemented to resolve the physical phenomena that occur in the sub-grid length scales [21], [39]. The sub-grid models account for a wide range of physical phenomena that occur during the life cycle of a droplet, starting from the initial injection from the nozzle until its complete evaporation.

The injection of parcels was performed using the Reitz and Diwakar [41] model, which assumes the initial discrete spherical droplets ('blobs') to be the same size as the nozzle diameter. The droplet breakup process was modeled using the KH-RT model, widely used in high pressure DI sprays [28], [42], [43]. The KH-RT model is based on two separate mechanisms that occur during the primary and secondary phases of the breakup of droplets.

Kelvin-Helmholtz hydrodynamic instabilities dominate the primary breakup phase, attributed to the unstable waves of the droplet-air interface [41]. Moreover, the secondary breakup is mainly caused by the aerodynamic drag force between the droplets and the air on the tip of the spray, attributed to Rayleigh-Taylor instabilities [41]. In addition, the TAB model was utilized, which assumes the droplet distortion and breakup to be proportional to a spring-mass-damper system [24]. Hence, the foundation of the model is based upon the analogy of the following parameters:

- Spring force $\cong$ Droplet surface tension
- External force $\cong$ Aerodynamic drag force
- Damping force $\cong$ Viscosity force

Consequently, droplet breakup occurs when the external aerodynamic force surpasses the droplet's internal forces from surface tension and viscosity. The two breakup models were compared and evaluated based on spray penetration and breakup occurrence.

The spray droplets interact through collisions and coalescence. The No Time Counter (NTC) algorithm [44] estimated the collisions between droplets, while the model of Post and Abraham [45] predicted the post-collision outcome, including bouncing, stretching, reflective separation, and coalescence. The droplet aerodynamic drag force was modeled using a dynamic drag model [46]. Lastly, the evaporation model is based on the Frossling correlation, assuming a uniform temperature distribution within each individual droplet [30], [47]. The correlation provides a link between the Reynolds (Re) and Schmidt (Sc) numbers with the Sherwood (Sh) number of the droplet. The Sherwood number quantifies the mass transfer rate from the droplet to the ambient environment playing a fundamental role in the evaporation process. Hence, the droplet radius rate of change is calculated as follows:

$$\frac{\mathrm{d}r_0}{\mathrm{d}t} = -\frac{\alpha_{spray}\rho_g D}{2\rho_l r_0} B_d Sh_d \qquad (11)$$

where r_0 is the initial drop radius, α_{spray} is a user-specified scaling mass transfer coefficient, D is the mass diffusivity, ρ_g and ρ_l are the gas and liquid densities respectively, and B_d is the fraction of vapour's mass fraction at the drop surface to the vapour mass fraction of the droplet. The Frossling correlation estimates the Sherwood number (Sh) as indicated by the following equation:

$$Sh_d = (2.0 + 0.6 {Re_d}^{\frac{1}{2}} Sc^{\frac{1}{3}}) \ln \frac{1 + B_d}{B_d} \qquad (12)$$

where Re_d is the droplet Reynolds number and Sc is the Schmidt number of air. The numerical models utilised in the computational study are summarised in Table 1.

Table 1: Numerical models

Physical Phenomena	**Numerical Models**
Fluid Flow	Navier Stokes, density-based solver [30]
Turbulence	RNG and Standard $k-\epsilon$ model [37]
Droplet Injection	Blob model [41]
Liquid Breakup	KH-RT model [28] & TAB model [24]
Droplet Drag Force	Dynamic Drag Model [46]
Droplet Collision	NTC model [44]
Droplet Coalescence	Post Collision Outcome model [45]
Droplet Evaporation	Frossling correlation-based model [30]

4 PORT FUEL INJECTION CONDITION STUDY

The employed numerical CFD study was based on the conditions reported in the experimental methanol PFI study by Liu, Chen, Su, *et al.* [15]. In their experiments, the authors utilized backlight imaging and high-speed photography to capture the spray morphology of methanol under low injection pressure conditions (constant $6\,\mathrm{bar}$ injection pressure). The study deployed a 14-hole injector with the intention of investigating the effect of varied ambient and fuel temperatures and ambient pressures on spray penetration. Based on their experimental study, Liu, Chen, Su, *et al.* [15] concluded that higher ambient and fuel temperatures result in faster evaporation time and larger penetration and cone angle.

4.1 Computational Study Initial & Boundary Conditions

The validation of the CFD model originates from the reported experimental spray penetration length under the $2\,\mathrm{bar}$ ambient air pressure and $25\,^{\circ}\mathrm{C}$ ambient air temperature condition [15]. Moreover, for the optimal performing model, a brief comparison of the $1\,\mathrm{bar}$ and $2.5\,\mathrm{bar}$ cases was conducted to demonstrate the robustness of the method. The selection of these ambient pressure conditions was closely related to the intake manifold conditions of turbocharged marine engines.

Detailed information about the initial conditions is presented in Table 2. The modeling included assumptions about the injected mass and nozzle di-

ameter, while the injector was modeled as a single-nozzle. These quantities have a significant influence on the spray structure and penetration. Therefore, their selection was conducted through trial and error resulting in a rational spray penetration prediction. Moreover, the order of magnitude of the values was in the context of automotive injection quantities and nozzle diameters [48]–[50]. The nozzle hydraulic characteristics were also tuned to match the experimental injection pressure.

Table 2: Low pressure PFI case conditions

Item	Value	Unit
Ambient Pressure	2	[bar]
Injection Duration	10	[ms]
Injection Pressure	6	[bar]
Injection Quantity (Assumed)	4.67	[mg]
Ambient Temperature	25	[°C]
Fuel Temperature	25	[°C]
Nozzle Diameter (Assumed)	0.15	[mm]
Nozzle Discharge Coefficient	0.87	[]

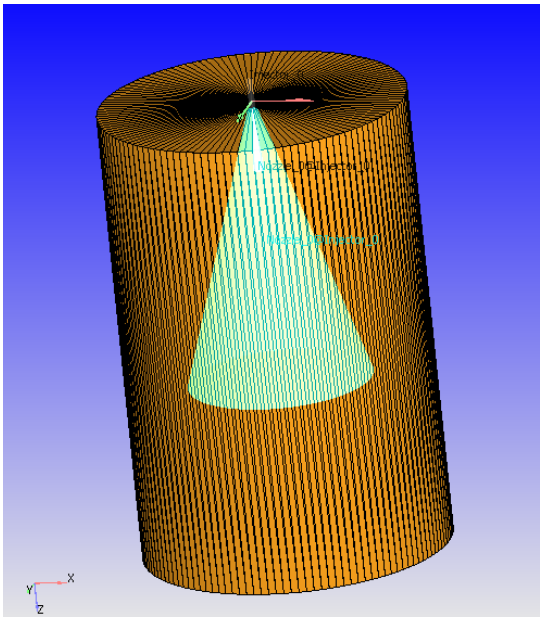

Figure 1: Simulation control volume

In this study, a cylindrical shaped control volume was adopted for the numerical computations (fig. 1) with a $60\,\mathrm{mm}$ radius and $180\,\mathrm{mm}$ height. The dimensions of the geometry were chosen in accordance with the literature of CFD spray studies for marine engines [20], [21]. The boundaries of the control volume were set as a wall-type condition with Neumann boundary conditions for the temperature and the turbulent kinetic energy. The numerical results considered 95% of liquid fuel mass fraction for calculating the liquid penetration. In the experiment, the liquid penetration was regarded as the vertical distance between the nozzle and the identified spray edge [15]. Moreover, the liquid penetration definition was slightly different between experimental and numerical data. However, the error in the comparison was sufficiently smaller than the other induced experimental uncertainties.

4.2 Mesh Convergence Study

A coarse mesh was employed with a uniform mesh grid having a base cell size of $4\,\mathrm{mm}$. The mesh grid was refined in the spray cone region to better resolve the flow field and the interactions between the droplets and the ambient air while keeping the overall cell count low for faster computation. As depicted in light green color in Fig. 1, the finer grid area encloses the cone of the spray area where the refinement was performed.

A grid convergence study was conducted for both turbulence models. Five different uniform cell sizes were tested for the spray cone area, ranging from $2\,\mathrm{mm}$ to $0.125\,\mathrm{mm}$. The liquid penetration length was monitored as the criterion for the convergence of the CFD model. The comparison with the liquid penetration results from the experiment showcased that the $0.5\,\mathrm{mm}$ grid was the most adequate for the study, aligning with spray-mesh guidelines from the literature [51]. Hence, the $0.5\,\mathrm{mm}$ grid was selected as the balanced trade-off for maintaining a grid-convergent and computationally viable mesh for the LE coupling.

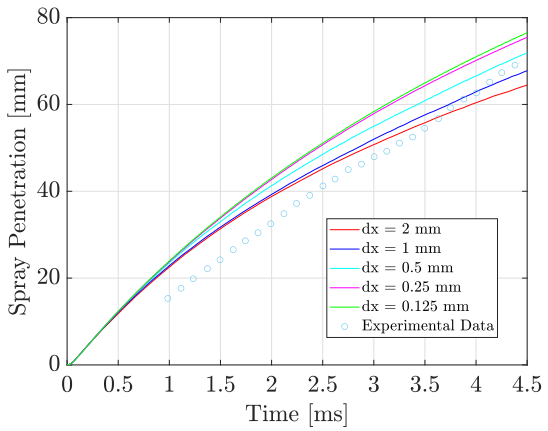

Figure 2: Grid convergence study

5 RESULTS & DISCUSSION

The comparison of the turbulence models demonstrated that the RNG $k-\epsilon$ is overpredicting spray penetration, aligning with the recommendations from diesel spray literature [20]. Therefore,

the Standard $k-\epsilon$ model coupled with the TAB liquid breakup model yielded reasonable predictions of the experimental liquid penetration values, accounting for the inherent uncertainties and unknowns in the experimental study (fig. 3).

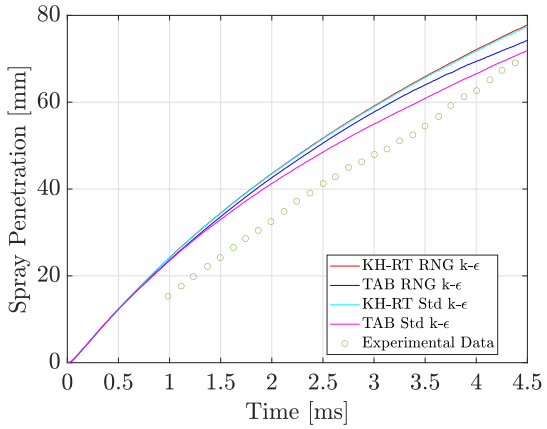

Figure 3: Influence of turbulence model & droplet breakup model on spray penetration

Moreover, in fig. 4, the coupling of the TAB model with the Standard $k-\epsilon$ turbulence model demonstrated satisfactory predicting capabilities for the other ambient pressures from the paper. However, accurately tuning the CFD model is impossible due to incomplete information on the reported experimental conditions. The primary objective of this study is to compare the droplet breakup model rather than assess the predictive capability of the numerical method. Therefore, the obtained computational results were considered rational for the scope of this research.

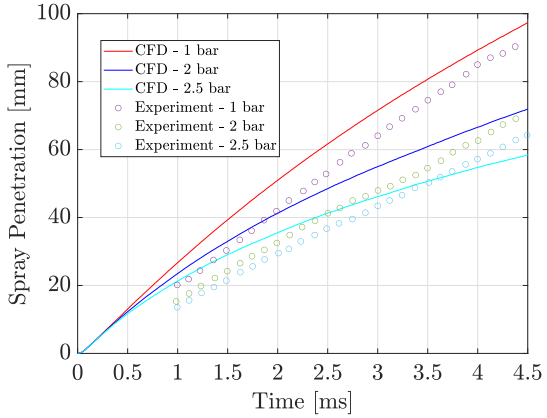

Figure 4: CFD model results for different ambient pressure conditions

5.1 Comparison of Droplet Breakup Model

In the section, the results considering the outcome of the droplet breakup model are demonstrated. Since there is a significant difference in the liquid penetration length between the TAB and the KH-RT models, this will greatly impact the resulting droplet sizes after breakup occurrence and, thus, the evaporation rate and the mixture fraction. Fig. 5 illustrates the Sauter Mean Diameter (SMD)[1], calculated for the entire spray structure, using each breakup model. The results indicate that the KH-RT model does not predict the occurrence of rational droplet breakup since the SMD remains approximately constant.

The opposite happened for the TAB model, demonstrating the presence of lower mean diameter length scales. Consequently, the higher SMD in the KH-RT model justifies the difference in the liquid penetration length due to the higher momentum of the larger droplets. It is also worth noting that the KH-RT model exhibited a slight increase in SMD due to droplet coalescence.

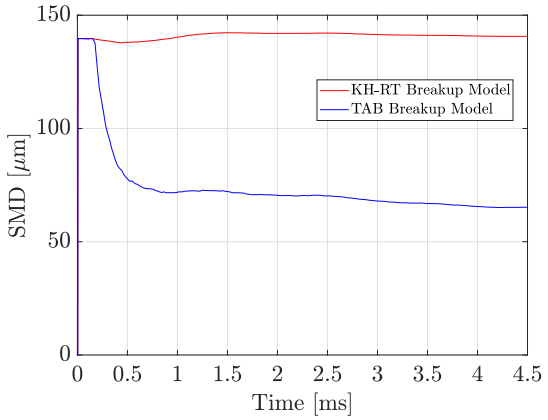

Figure 5: Comparison of Droplet Breakup Model (non evaporating conditions) - SMD

5.2 Evaporating Conditions

The conditions reported in this paper include a relatively low ambient temperature, which hinders spray evaporation. In this section, a set of higher ambient and fuel temperature conditions was examined to facilitate evaporation of the methanol spray (shown in Table 3).

[1]The SMD is interpreted as the diameter of a drop having the same volume to surface area ratio as the entire spray [52].

Table 3: Evaporating conditions

Item	Value	Unit
Ambient Temperature	100	[°C]
Fuel Temperature	80	[°C]

The previous study's adopted models were used to examine the performance of the KH-RT and TAB breakup models under evaporating condition. As before, the KH-RT model predicted higher liquid penetration length (fig. 6) due to diminished droplet breakup occurrence (fig. 7). This difference in penetration length was more pronounced due to the decreased evaporation rate of large droplets in the KH-RT case.

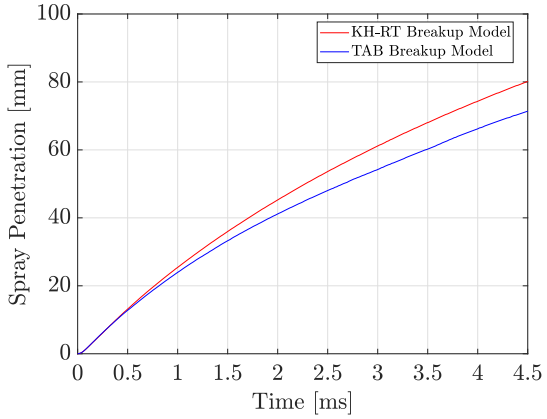

Figure 6: Comparison of Droplet Breakup Model (under evaporating conditions) - Spray Penetration

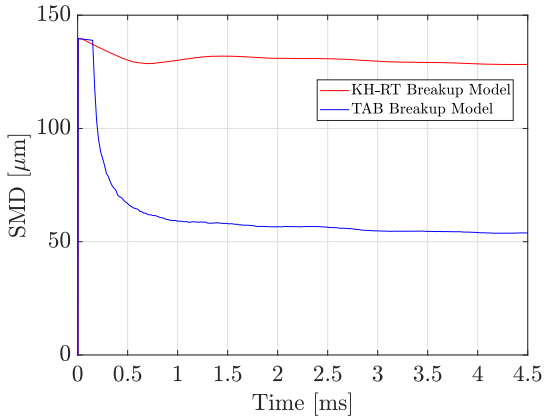

Figure 7: Comparison of Droplet Breakup Model (under evaporating conditions) - SMD

Figure 8 illustrates a comparison of 3D droplet diameters between the droplet breakup models. The plot displays the individual diameters of each particle in the computational domain. The comparison highlights the discrepancy in the SMD, with droplet sizes ranging from 120 µm to 160 µm for the KH-RT model. In contrast, the TAB model exhibits smaller droplet sizes ranging from 40 µm to 80 µm microns.

As mentioned before, the difference in the outcome particles after droplet breakup significantly influences the evaporation rate. Mass fraction contours illustrate the extent of methanol evaporation and mixing with the surrounding air. Fig. 10 confirms higher predicted mass fractions for the TAB case, supporting the initial hypothesis of evaporation prediction.

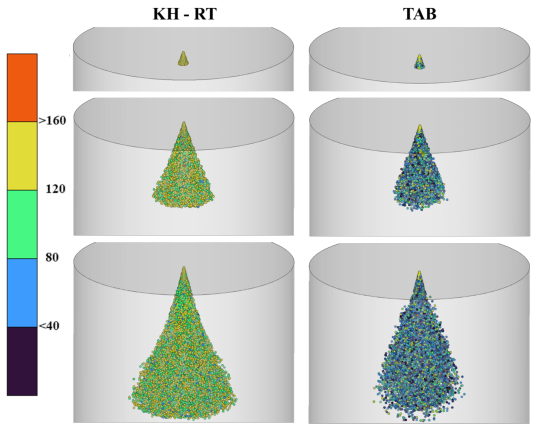

Figure 8: Droplet Diameter comparison, for $t = 0.27, 2, 4.5$ ms - Diameter in μm.

Furthermore, fig. 9 presents the total mass of evaporated methanol. This result emphasizes the importance of selecting the appropriate droplet breakup model for simulating low pressure PFI sprays.

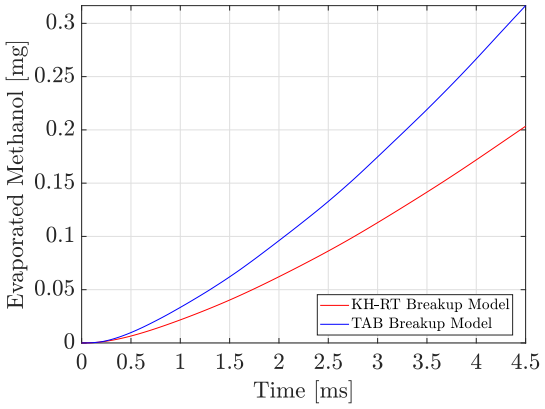

Figure 9: Comparison of Droplet Breakup Model (under evaporating conditions) - Evaporated Methanol

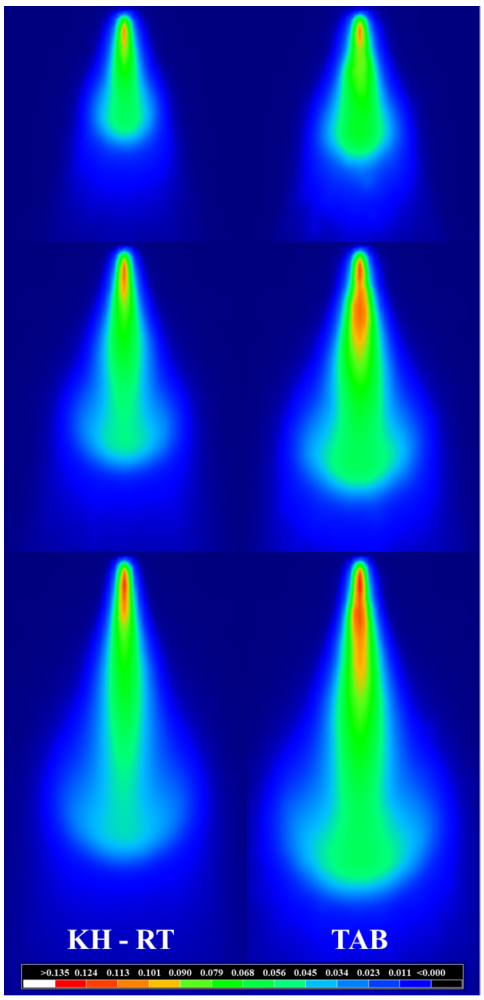

Figure 10: Methanol mass fraction contours plot - Comparison between KH-RT and TAB model, for $t = 1.5$, 3.0, and 4.5 ms.

Finally, examining the We number during the initial phase of the injection is crucial. According to O'Rourke and Amsden [24], the critical We number for vibrational breakup is 12. Therefore, it is important to maintain a value below this threshold for the TAB model's validity. Since the liquid jet is injected into an ambient environment with zero initial velocity, the drag force will naturally decelerate the droplets, resulting in a decrease in their We number. Consequently, the initial velocity of the "blobs" exiting the nozzle is the primary condition for selecting the appropriate breakup model. In fig. 11, the visualization of the We number confirms the rationality of choosing the TAB model.

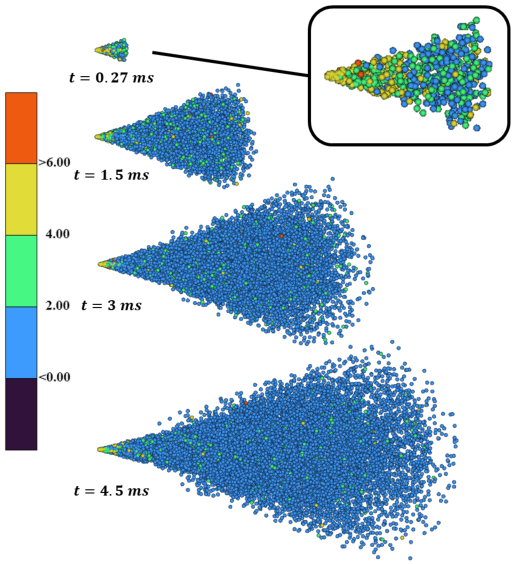

Figure 11: Weber number in TAB model injection

6 CONCLUSIONS

This study aimed to conduct a preliminary assessment of the impact of spray submodels on CFD spray predictions. The study examined the influence of the droplet breakup mechanism and the turbulence model under low injection pressure. The KH-RT and TAB models were compared, along with an investigation into the performance of the RNG and Standard $k - \epsilon$ turbulence models. The results demonstrated a satisfactory prediction of the spray penetration, consistent with experimental observations reported by Liu, Chen, Su, *et al.* [15]. This analysis provides a valuable initial step towards selecting appropriate models for maritime methanol PFI spray simulations. Therefore, the utilization of the TAB breakup model and the Standard $k - \epsilon$ model provided rational predictions for PFI conditions, which is in line with the previous findings in the literature [20], [25], [26]. This simulation step could be instrumental in shaping future studies in marine engines encompassing predictive CFD modeling to assess atomization quality and minimize wall wetting. Moreover, this study's predicted droplet sizes demonstrated poor spray atomization under low injection pressure in intake port conditions. Hence, the relatively large droplets hindered the evaporation process and increased risk of wall wetting of the inlet manifold.

In conclusion, this study highlights the importance of investigating spray submodels for PFI conditions. Understanding the specific droplet breakup mode is crucial for selecting an appropriate modeling technique that accurately captures the underlying physics. Specifically, in low-pressure PFI

sprays, the dominant breakup mode is characterized by droplet vibration, which can be effectively modeled using the TAB model. CFD analysis confirmed this by observing low Weber numbers indicating the prevalence of vibrational breakup. Additionally, the TAB model outperformed the KH-RT model in capturing breakup behavior under these conditions. However, further investigation is required to assess the limitations of the TAB model in PFI scenarios. This investigation should consider the critical Weber number and compare the droplet breakup regimes predicted by each model. Specifically, the evaluation should be conducted under modified droplet breakup regimes at higher injection pressures in PFI conditions. Lastly, appropriate experimental data, including spray images and SMD measurements, are necessary to sufficiently validate the proposed modeling approach.

ACKNOWLEDGEMENTS

The present research is part of the MENENS project (Methanol als Energiestap Naar Emissieloze Nederlandse Scheepvaart). The project is funded by the Netherlands Enterprise Agency (RVO: Rijksdienst voor Ondernemend Nederland). We would like to thank Convergent Science [29], and BETA CAE Systems [53] for offering their software (CONVERGE, ANSA & META) and their technical support for the accomplishment of this research. ANSA was used for geometry creation and pre-processing of the CFD model, CONVERGE for the CFD simulations, and META for post-processing and visualisation of the results.

REFERENCES

[1] *International Maritime Organization: Fourth Greenhouse Gas Study 2020*, 2020. [Online]. Available: https://www.imo.org/en/OurWork/Environment/Pages/Fourth-IMO-Greenhouse-Gas-Study-2020.aspx.

[2] D. G. Kessel, "Global warming—facts, assessment, countermeasures," *Journal of Petroleum Science and Engineering*, vol. 26, no. 1-4, pp. 157–168, 2000.

[3] L. C. Law, B. Foscoli, E. Mastorakos, and S. Evans, "A comparison of alternative fuels for shipping in terms of lifecycle energy and cost," *Energies*, vol. 14, no. 24, p. 8502, 2021.

[4] M. Perčić, N. Vladimir, and A. Fan, "Life-cycle cost assessment of alternative marine fuels to reduce the carbon footprint in short-sea shipping: A case study of Croatia," *Applied Energy*, vol. 279, Dec. 2020. (visited on 05/23/2022).

[5] R. D. Reitz, H. Ogawa, R. Payri, *et al.*, "IJER Editorial: The future of the internal combustion engine," *International Journal of Engine Research*, 2020. DOI: 10.1177/1468087419877990.

[6] C. J. McKinlay, S. R. Turnock, and D. A. Hudson, "Route to zero emission shipping: Hydrogen, ammonia or methanol?" *International Journal of Hydrogen Energy*, vol. 46, no. 55, pp. 28 282–28 297, 2021.

[7] M. Tuner, "Review and Benchmarking of Alternative Fuels in Conventional and Advanced Engine Concepts with Emphasis on Efficiency, CO2, and Regulated Emissions," *SAE Technical Papers*, 2016.

[8] A. Ait Allal, K. Mansouri, M. Youssfi, and M. Qbadou, "Toward an evaluation of marine fuels for a clean and efficient autonomous ship propulsion energy," *Materials Today: Proceedings*, vol. 13, pp. 486–495, 2019. (visited on 05/23/2022).

[9] S. Verhelst, J. W. Turner, L. Sileghem, and J. Vancoillie, "Methanol as a fuel for internal combustion engines," *Progress in Energy and Combustion Science*, vol. 70, pp. 43–88, Jan. 2019.

[10] A. D. Korberg, S. Brynolf, M. Grahn, and I. R. Skov, "Techno-economic assessment of advanced fuels and propulsion systems in future fossil-free ships," *Renewable and Sustainable Energy Reviews*, vol. 142, May 2021. (visited on 07/15/2022).

[11] J. Singh, A. Dhar, and P. Kumar, "Methanol Fuel in Compression Ignition Engines," in *Energy, Environment, and Sustainability*, Springer Nature, 2022, pp. 71–101. (visited on 05/19/2022).

[12] J. Dierickx, J. Verbiest, T. Janvier, J. Peeters, L. Sileghem, and S. Verhelst, "Retrofitting a high-speed marine engine to dual-fuel methanol-diesel operation: A comparison of multiple and single point methanol port injection," *Fuel Communications*, vol. 7, p. 10, 2021.

[13] B. Zincir and C. Deniz, "Methanol as a Fuel for Marine Diesel Engines," in *Energy, Environment, and Sustainability*, Springer Nature, 2021, pp. 45–85. (visited on 05/23/2022).

[14] M. Pipicelli, G. Di Luca, R. Ianniello, A. Gimelli, and C. Beatrice, "Alcohol Fuels in Compression Ignition Engines," in *Energy, Environment, and Sustainability*, Springer Nature, 2022, pp. 9–31.

[15] K. Liu, C. Chen, M. Su, *et al.*, "Experimental study of the macroscopic characteristics of methanol low-pressure injection spray," en, *International Journal of Energy Research*, er.8625, Aug. 2022. (visited on 11/01/2022).

[16] Y. Gong, S. Liu, and Y. Li, "Investigation on methanol spray characteristics," *Energy and Fuels*, vol. 21, no. 5, pp. 2991–2997, Sep. 2007.

[17] A. Matamis, S. Lonn, M. Tuner, O. Andersson, and M. Richter, "Optical Characterization of Methanol Sprays and Mixture Formation in a Compression-Ignition Heavy-Duty Engine,"

en, Sep. 2020, pp. 2020–01–2109. (visited on 09/01/2022).

[18] A. Ghosh, P. Boggavarapu, and R. V. Ravikrishna, "MEASUREMENT OF LIQUID AND VAPOR PENETRATION OF EVAPORATING METHANOL SPRAYS," *Atomization and Sprays*, vol. 30, no. 10, pp. 741–757, 2020.

[19] Y. Wang, P. Dong, W. Long, *et al.*, "Characteristics of Evaporating Spray for Direct Injection Methanol Engine: Comparison between Methanol and Diesel Spray," *Processes*, vol. 10, no. 6, p. 1132, Jun. 2022. (visited on 07/13/2022).

[20] H. Li, T. Beji, and S. Verhelst, "Improving the calculation of evaporating sprays for medium-speed marine-engine-like conditions," *Atomization and Sprays*, vol. 31, no. 8, 2021.

[21] N. Maes, N. Dam, B. Somers, T. Lucchini, G. D'Errico, and G. Hardy, "Experimental and numerical analyses of liquid and spray penetration under heavy-duty diesel engine conditions," *SAE International Journal of Fuels and Lubricants*, vol. 9, no. 1, pp. 108–124, 2016.

[22] R. Reitz *et al.*, "Modeling atomization processes in high-pressure vaporizing sprays," *Atomisation and Spray technology*, vol. 3, no. 4, pp. 309–337, 1987.

[23] L. M. Pickett, J. Manin, R. Payri, M. Bardi, and J. Gimeno, "Transient rate of injection effects on spray development," SAE Technical Paper, Tech. Rep., 2013.

[24] P. J. O'Rourke and A. A. Amsden, "The tab method for numerical calculation of spray droplet breakup," SAE Technical Paper, Tech. Rep., 1987.

[25] G. C. Papageorgakis and D. N. Assanis, "A spray breakup model for low injection pressures," *International communications in heat and mass transfer*, vol. 23, no. 1, pp. 1–10, 1996.

[26] F. Balduzzi, G. Vichi, L. Romani, *et al.*, "Development of a low pressure direct injection system for a small 2s engine. part i-cfd analysis of the injection process," *SAE International Journal of Engines*, vol. 8, no. 4, pp. 1885–1897, 2015.

[27] D. D. Joseph, J. Belanger, and G. Beavers, "Breakup of a liquid drop suddenly exposed to a high-speed airstream," *International Journal of Multiphase Flow*, vol. 25, no. 6-7, pp. 1263–1303, 1999.

[28] J. C. Beale and R. D. Reitz, "Modeling spray atomization with the kelvin-helmholtz/rayleigh-taylor hybrid model," *Atomization and sprays*, vol. 9, no. 6, 1999.

[29] *CONVERGE CFD Software Website*, 2023. [Online]. Available: `https://convergecfd.com/`.

[30] Convergent Science Inc, *CONVERGE MANUAL v3.0*. 2022.

[31] J. H. Ferziger, M. Perić, and R. L. Street, *Computational methods for fluid dynamics*. Springer, 2002, vol. 3.

[32] P. K. Kundu, I. M. Cohen, and D. R. Dowling, *Fluid mechanics*. Academic press, 2015.

[33] R. I. Issa, "Solution of the implicitly discretised fluid flow equations by operator-splitting," *Journal of computational physics*, vol. 62, no. 1, pp. 40–65, 1986.

[34] A. Horvath, "Redlich-kwong equation of state: Review for chemical engineering calculations," *Chemical Engineering Science*, vol. 29, no. 5, pp. 1334–1340, 1974.

[35] D. H. P. C. C. (DHPC), *DelftBlue Supercomputer (Phase 1)*, 2022. [Online]. Available: `https://www.tudelft.nl/dhpc/ark/delftbluephase1`.

[36] W. Gropp, E. Lusk, N. Doss, and A. Skjellum, "A high-performance, portable implementation of the mpi message passing interface standard," *Parallel computing*, vol. 22, no. 6, pp. 789–828, 1996.

[37] Z. Han and R. D. Reitz, "Turbulence modeling of internal combustion engines using rng κ-ε models," *Combustion science and technology*, vol. 106, no. 4-6, pp. 267–295, 1995.

[38] S. B. Pope and S. B. Pope, *Turbulent flows*. Cambridge university press, 2000.

[39] C. Baumgarten, *Mixture formation in internal combustion engines*. Springer Science & Business Media, 2006.

[40] S. Subramaniam, "Lagrangian–eulerian methods for multiphase flows," *Progress in Energy and Combustion Science*, vol. 39, no. 2-3, pp. 215–245, 2013.

[41] R. D. Reitz and R. Diwakar, "Structure of high-pressure fuel sprays," *SAE transactions*, pp. 492–509, 1987.

[42] H. Li, R. Verschaeren, G. Decan, and S. Verhelst, "Evaluation of breakup models for marine diesel spray simulations," in *29th Conference on Liquid Atomization and Spray Systems (ILASS-Europe 2019)*, Centre pour la Communication Scientifique Directe, 2020.

[43] R. D. Reitz, "Mechanism of breakup of round liquid jets," *Encyclopedia of fluid mechanics*, vol. 10, 1986.

[44] D. P. Schmidt and C. J. Rutland, "A new droplet collision algorithm," *Journal of Computational Physics*, vol. 164, no. 1, pp. 62–80, 2000.

[45] S. L. Post and J. Abraham, "Modeling the outcome of drop–drop collisions in diesel sprays," *International Journal of Multiphase Flow*, vol. 28, no. 6, pp. 997–1019, 2002.

[46] A. B. Liu, D. Mather, and R. D. Reitz, "Modeling the effects of drop drag and breakup on fuel sprays," *SAE Transactions*, pp. 83–95, 1993.

[47] R. Miller, K. Harstad, and J. Bellan, "Evaluation of equilibrium and non-equilibrium evaporation models for many-droplet gas-liquid flow simulations," *International journal of multiphase flow*, vol. 24, no. 6, pp. 1025–1055, 1998.

[48] T. Lucchini, G. D'Errico, D. Ettorre, and G. Ferrari, "Numerical investigation of non-reacting and reacting diesel sprays in constant-volume ves-

sels," *SAE International Journal of Fuels and Lubricants*, vol. 2, no. 1, pp. 966–975, 2009.

[49] *Engine Combustion Network Spray-G Conditions*, 2023. [Online]. Available: https://ecn.sandia.gov/gasoline-spray-combustion/target-condition/spray-g-operating-condition/.

[50] *Engine Combustion Network*, 2023. [Online]. Available: https://ecn.sandia.gov/.

[51] T. Lucchini, G. D'Errico, and D. Ettorre, "Numerical investigation of the spray–mesh–turbulence interactions for high-pressure, evaporating sprays at engine conditions," *International Journal of Heat and Fluid Flow*, vol. 32, no. 1, pp. 285–297, 2011.

[52] S. McAllister, J.-Y. Chen, A. C. Fernandez-Pello, S. McAllister, J.-Y. Chen, and A. C. Fernandez-Pello, "Droplet evaporation and combustion," *Fundamentals of Combustion Processes*, pp. 155–175, 2011.

[53] *BETA CAE Systems Website*, 2023. [Online]. Available: https://www.beta-cae.com/.